Bioprinting 16 (2019) e00056

Contents lists available at ScienceDirect

Bioprinting

journal homepage: www.elsevier.com/locate/bprint

A combinatorial approach: Cryo-printing and electrospinning hybrid scaffolds for cartilage tissue engineering

N. Munir, A. McDonald, A. Callanan *

School of Engineering, Institute for Bioengineering, University of Edinburgh, Scotland, United Kingdom

ARTICLE INFO

Keywords:
Cartilage
Cryo-printing
Directional freezing
Phase separation
Electrospinning
Mesenchymal stem cells

ABSTRACT

Osteoarthritis is the predominant form of arthritis and is a leading cause of disability. Tissue engineered scaffolds are showing great promise for the treatment of cartilage defects. The cartilage consists of a complex architecture, which is greatly responsible for its properties and functions. In this study, highly porous multizone scaffolds were fabricated using both cryo-printing and electrospinning. The developed multizone scaffolds successfully mimic the complex structure of the collagen fibre orientation in the native cartilage. MSC were seeded onto the multizone scaffolds. Cell viability, DNA quantification and fluorescence staining demonstrated that these scaffolds allow MSC attachment and viability after 4 weeks of in *vitro* culture. Moreover, a key chondrogenesis factor, glycosaminoglycan, was maintained over 4 weeks of culture. Compressive properties of the multizone scaffolds were significantly lower in comparison to the phase separated control, making it mechanically suitable for the cartilage. Overall, this study produced multizone scaffolds which express a complex structure similar to that of the native cartilage and the results demonstrate the ability of the multizone scaffolds to act as platforms for MSC attachment and survival, highlighting the potential within cartilage tissue engineering.

1. Introduction

Osteoarthritis is the most common articular disease and is a leading cause of disability [1]. Current non-surgical and surgical therapies have failed to halt the progression of osteoarthritis and it's prevalence is on the rise. Surgical treatments including abrasion, arthromplasty, osteochondral grafting and total knee arthroplasty are employed but success is hindered with high failure rates. Autologous chondrocyte implantation (ACI) has been increasingly used over the last 20 years but its use is associated with high costs, weeks of cell culture, and two operations [2–6]. Microfracture is a highly regarded technique and is considered the 'gold standard' for treatment of cartilage defects. It is a low cost and minimally invasive procedure, however, this technique results in the formation of fibrocartilage due to the lack of guidance for cellular migration and structural support [7–10]. In order to overcome these hurdles, tissue engineered scaffolds have gained widespread attention for their potential to aid in cartilage repair with many achieving preliminary success [6,11–13]. Various cells and scaffold fabrication techniques have been used for engineering cartilage tissue [14–21].

The use of mesenchymal stem cells (MSC) to repair cartilage defects is a promising avenue as MSC possess the ability to undergo differentiation into chondrocytes under the influence of appropriate biological cues *in vitro* [22–24]. Previously, MSC cultured in cell pellets exhibited chondrogenic properties [25,26], however, the inadequate mechanical properties limit the use as systems for cartilage repair [27]. On the other hand, biomaterial scaffolds have shown the potential to provide required mechanical properties and relevant platforms for MSC differentiation [23,28].

The physical architecture of scaffolds is a key parameter which regulates cell activity [28]. Native cartilage is characterised with collagen fibres in various orientations and this complex structure has a vital role in physiological and mechanical functions of the cartilage [3,29]. The unique composition and three layered structure of the cartilage has been the focus of a limited number of previous studies. Multi-layered constructs that mimic various characteristics of the native cartilage have been previously developed [3,11,12,29–31]. One approach is to incorporate biological components of the native cartilage into layered scaffolds. An example is 3D bioprinted multi-layered osteochondral constructs consisting of various ECM materials which allowed the production of neo cartilage [30]. In regards to mimicking cartilage architecture, bi- or multi-layered scaffolds have been constructed using either one or two scaffold fabrication techniques. These scaffolds presented

* Corresponding author. Institute for Bioengineering (IBioE), The School of Engineering, The University of Edinburgh, Faraday Building, King's Buildings, Edinburgh, UK.
E-mail address: Anthony.Callanan@ed.ac.uk (A. Callanan).

https://doi.org/10.1016/j.bprint.2019.e00056
Received 21 January 2019; Received in revised form 31 May 2019; Accepted 1 July 2019

region specific variations in mechanical properties, chondrocyte number and cartilage ECM production [11,12,31]. Similarly, scaffolds with biomimetic pore architecture have been developed, using directional freezing, and these scaffolds demonstrated pore dependant mechanical anisotropy [29].

Recently, we developed a cryo-printer which is a modified 3D printer that prints directly onto a -40 °C surface. This technique allows the printed solution to undergo phase separation and directional freezing resulting in columnar pores, similar to the parallel structure of the deep zone layer of the native cartilage [32]. To recreate the complex multizonal architecture of the native cartilage, cyro-printing can be used in combination with other scaffold fabrication techniques. For instance, biodegradable polymeric electrospun nanofibers have previously been shown to be morphologically similar to natural extracellular matrix, thus, it has been widely used in tissue engineering. They exhibit porosity (>90%) and successfully promotes cell attachment and growth [12,14]. However, electrospun nanofibers usually exhibit poor mechanical properties, limiting their use in load-bearing tissue engineering applications, such as cartilage [33,34].

The present study combined the use of cryo-printing and electrospinning to develop multizone scaffolds that recreate the complex architecture of the native cartilage. The scaffold contains three distinct zones, each of which mimics the zonal architecture of the native cartilage. Multizone scaffolds were directly compared to phase separated (P/S) and electrospun (ESP) controls.

2. Materials and methods

2.1. Materials

All materials were purchased from Sigma Aldrich unless stated otherwise.

2.2. Multizone scaffold fabrication

The bottom zone of the multizone scaffold was fabricated using cryo-printing, which involves printing of an 8% w/v Polycaprolactone (PCL)/1, 4-Dioxane solution directly onto a cold plate set at -40°C, as described in previous literature [32]. This layer was printed in a helix shape. Print head temperature, speed, and solution flow rate were set to 45°C, 0.5 mm/s and 1.25 ml/h, respectively. Printed scaffolds were further frozen at -80°C overnight and then freeze dried overnight (FreeZone 4.5 freeze-drier, Labconco). The middle and top layers were composed of random and aligned electrospun fibres, respectively. Both layers were created using 8% w/v PCL in HFIP at 13 kV with a flow rate of 2 ml/h, needle bore of 0.8 mm and with a needle to mandrel distance of 11 cm. The mandrel rotation speed was 200RPM for randomly orientated fibres and 2400RPM for aligned fibres. As controls to the multizone scaffolds, P/S and ESP scaffolds were used. The P/S scaffold were made from PCL/1, 4-Dioxane solution which was put into pre cooled moulds on the cold plate set at -40°C. The ESP controls consisted of both randomly orientated and aligned fibres and were made using the electrospinning parameters described above.

2.3. Plasma coating

Scaffolds were cut into 10 mm discs, soaked in 70% ethanol for 30mins, rinsed thrice in PBS for 15mins each and then freeze dried overnight in a FreeZone 4.5 freeze-drier (Labconco). Scaffolds were then plasma coated (Harrick Plasma) at 26.6 W, 500mTorr for 3mins. Immediately after coating, scaffolds were immersed into 1% v/v antibiotic/antimycotic solution overnight.

2.4. Scaffold morphology characterisation

Scanning electron microscope (SEM), Hitachi S4700, was used to characterise scaffold morphology. Prior to imaging, scaffolds were coated with gold and palladium alloy (Polaron Sputtercoater). Using SEM images and image J (NIH) strand diameter, pore size and fibre diameter were analysed.

2.5. Isolation and culture of primary rat MSC

Primary MSC were isolated from a 4 week old female Sprague Dawley rat. Briefly, the femur was extracted and excess tissue was removed. The femur was then soaked in 70% ethanol for 5mins and then PBS for 2mins. Both ends of the femur were cut and the bone marrow was flushed out with media using a needle and syringe. Isolated cells were cultured (37°C, 5% CO_2) in T75 flasks in α-mem supplemented with 10% v/v FBS and 1% v/v antibiotic/antimycotic until confluent.

2.6. Scaffold seeding

Prior to seeding, scaffolds were soaked in chondrogenic media; high glucose DMEM supplemented with 50 µg/ml ascorbic acid, 50 µg/ml L-Proline, 0.1 mM sodium pyruvate, 10 ng/ml TGF-β3 (Biolegend), 1% ITS premix and 1% antibiotic/antimycotic. MSC were seeded onto all scaffolds (260,000 cells in 20 µl of media) and were allowed to adhere for 3 h at 37°C, 5% CO_2. After cell adhesion, 1.5 ml of chondrogenic media was added into each well and scaffolds were cultured for 24hr, 2 and 4 weeks at 37°C and 5% CO_2 with weekly media changes.

2.7. Scaffold seeding efficiency

Scaffold seeding efficiency was determined using Quant-iT™ PicoGreen™ dsDNA Assay Kit (ThermoFisher Scientific) and CellTiter-Blue cell viability assay (Promega). Scaffolds and tissue culture wells, seeded with 260,000 cells, were cultured for 24 h before performing these assays. For DNA quantification, 260,000 cells were immediately frozen and not seeded to use as controls.

2.8. Cell viability

Cell viability was assessed using CellTiter-Blue cell viability assay (Promega). Scaffolds were moved to new wells and were incubated with CellTiter-Blue working solution (5:1 media to assay) for 4 h at 37°C, 5% CO_2. Fluorescence measurements were analysed using a Modulus™ II microplate multimode reader at Ex 525 nm and Em 580–640 nm, n = 4.

2.9. DNA analysis

Scaffolds were freeze dried and digested in papain digest solution (2.5U/ml papain, 5 mM cysteine-HCl and 5 mM ethylenediaminetetraaceticacid in PBS) overnight at 65°C. Total DNA content of samples was analysed using Quant-iT™ PicoGreen™ dsDNA Assay Kit (ThermoFisher Scientific), according to the manufactures protocol. Fluorescence was read at Ex 480 nm and Em 510–570 nm using a microplate reader.

2.10. Glycosaminoglycan quantification

Glycosaminoglycan (GAG) content was assessed using the sulphated GAG assay kit (Blyscan, Biocolor Ltd), using the manufacturer's instructions. Samples were digested in papain (2.5U/ml papain, 5 mM cysteine-HCl and 5 mM ethylenediaminetetraaceticacid in PBS). The digested sample was mixed with Blyscan dye reagent composed of 1, 9-dimethyl- methylene blue for 30mins, and the unbound dye solution was removed by centrifugation. Bound dye was released from the insoluble GAG complex using the Blyscan dissociation reagent. Absorbance of samples was read at an excitation wavelength of 656 nm using a ModulusTM II microplate multimode reader. A standard curve was used to quantify total amount of GAG.

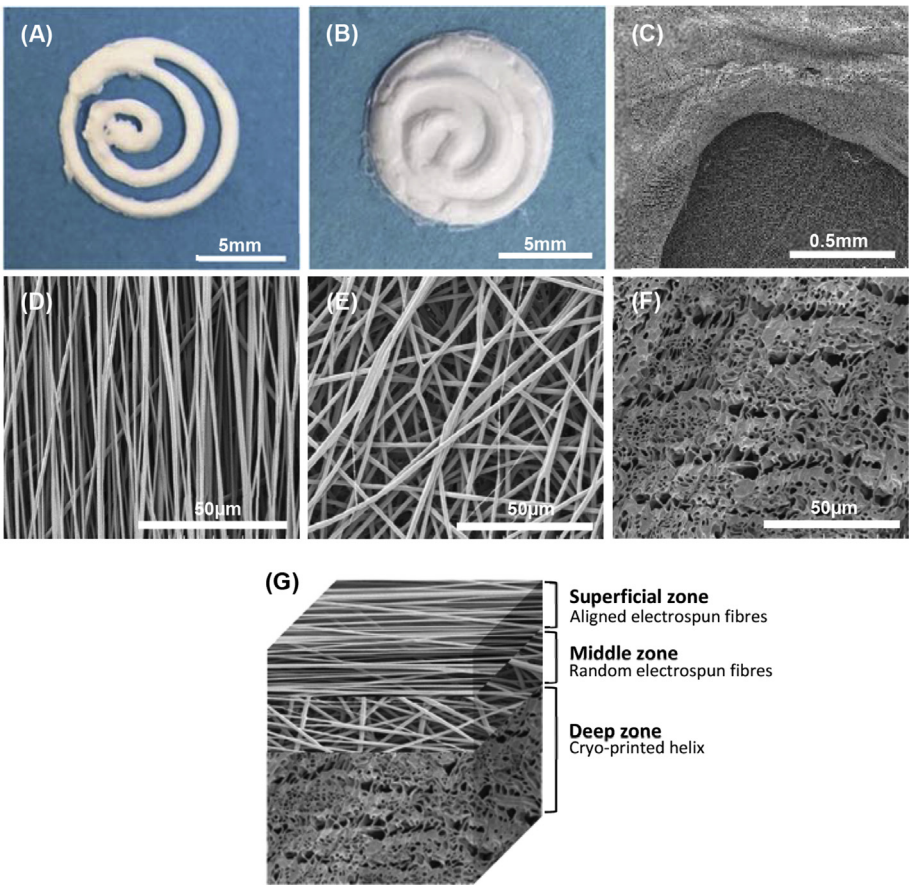

Fig. 1. Scaffold design and architecture. (A) Cryo-printed helix, bottom layer of multizone scaffold. (B) Multizone scaffold: Cryo-printed helix with electrospun middle and top layer. (C) SEM image of multizone scaffolds showing the bottom helix zone and middle randomly orientated fibres layer underneath it. (D) Top layer of multizone scaffold, aligned electrospun fibres. (E) Middle layer of multizone scaffold, randomly orientated fibres. (F) Helix bottom layer of multizone scaffold, porous surface. (G) Diagram illustrating the various layers of the multizone scaffold.(A).

2.11. Mechanical testing

Compression testing was performed using an Instron Model 3367 testing machine. Scaffolds were immersed in PBS prior to testing and were compressed to 30% strain at a crosshead speed of 0.5% strain/min. Young's modulus was calculated from the linear region of the stress-strain curve and incremental Young's modulus was analysed between 0 and 5, 5–10, 10–15 and 15–20% strains.

2.12. Scaffold staining

Fluorescent imaging was carried out at each time point to visualise cell attachment. Scaffolds were rinsed thrice in PBS and fixed in 4% v/v formalin in PBS overnight. Scaffolds were rinsed in PBS prior to permeabilisation in 0.2% Triton X-100 for 30mins. Scaffolds were then washed three times in PBS for 10mins each. Cells were stained with 1000X Phalloidin-iFluorTM514 conjugate (AAT Bioquest, Stratech) in PBS with 1% bovine serum albumin (1:1000) for 1hr. Scaffold washing was repeated three times in PBS for 10mins each. Cells were then stained with 300 nM 4′, 6-diamidino-2- phenylindole (DAPI) (Sigma-Aldrich, UK) in PBS for 10mins and scaffolds were rinsed in PBS for three 10mins washes. Stained scaffolds were then mounted on glass coverslips for imaging.

2.13. Multiphoton microscopy

A custom-built multi-photon microscope was used to acquire coherent anti-stokes Raman scattering (CARS) and two photon excitation fluorescence (TPEF) images. Seeded scaffolds stained with phalloidin and DAPI were imaged using CARS microscopy to detect the PCL fibres (2911 cm^{-1}) and at the same time exciting TPEF from the stained cells. Emission signals were separated to allow CARS and phalliodin signals to be acquired simultaneously. In specific, signals were separated using a dichroic filter cube consisting of a 649 nm dichroic, with 660/13 nm and 542/50 nm bandpass filters respectively. Using a second filter cube consisting of a 570 nm dichroic with a 454/50 nm bandpass filter, DAPI images were acquired consecutively. For image acquisition, a 25x/1.05 N A water immersion objective lens (XLPlan N, Olympus) with 75 mW and 115 mW at the sample for the 1064 nm and 812.6 nm beams was used, respectively.

In order to analyse cell growth in the void of the multizone scaffold, Z-stacks were taken at 2 μm intervals up to 450 μm into the sample. Maximum intensity projection images were then generated using icy and all slices were stacked in a single 2D image which allowed for visualisation of the boundary and growth of MSC on the inner cell layer.

2.14. Widefield epi-fluorescence microscopy

Acquisition of epi-fluorescence images, to evaluate attachment of phalloidin labelled cells on the multizone scaffold, was carried out using an inverted microscope (DMIRB, Leica) with a 5x/0.12 N A objective lens (N Plan, Leica). A metal halide lamp (LumenPro 200) with a 485/20 nm excitation band pass filter was used to illuminate the samples. In order to separate the fluorescence emission from the excitation source, a multi-band filter was set up (69300, Chroma). An Andor Zyla sCMOS camera was used to acquire the images, with an exposure time of 60 ms. A grid of images were obtained across the sample with a 20% overlap. Then the grid collection stitching plug-in (Fiji) was used to stitch individual images together to generate an image of the full scaffold. The camera, lamp and motorised sample stage (Prior) were all controlled using a micromanager v2.0.

2.15. Gene expression analysis

After 24hrs, 2 and 4 weeks, total RNA was extracted from scaffolds

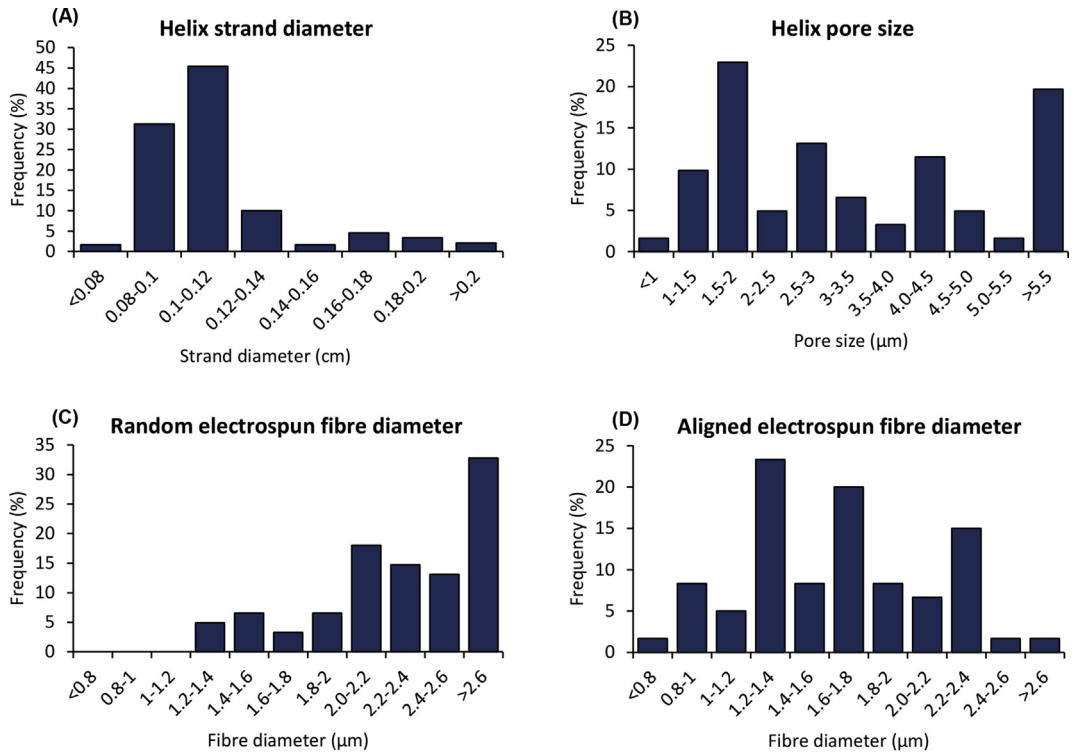

(E)

Fibre diameter (µM, mean±SD)	
Aligned fibres	1.57±0.50
Random fibres	2.34±0.74
Pore size (µM, mean±SD)	
Printed helix	3.62±0.74

Fig. 2. Scaffold morphology characterisation. (A) Printed helix, bottom layer of multizone scaffold, strand diameter analysis. (B) Printed helix, bottom layer of multizone scaffold, pore size analysis. (C) Randomly orientated fibres, middle layer of multizone scaffold, fibre diameter analysis. (D) Aligned fibres, top layer of multizone scaffold, fibre diameter analysis. (E) Table presenting mean fibre and pore sizes.

using Tri-reagent (ThermoFisher Scientific), chloroform and ethanol. RNA was purified using Qiagen's RNeasy spin column system, as previously described. RNA concentration was determined using absorbance at 260mn. cDNA was obtained from reverse transcription using the Promega's ImProm-II Reverse Transcription System. Quantitative real-time polymerase chain reaction (qPCR) was carried out on a LightCycler® 480 Instrument II (Roche Life Science). qPCR was performed using previously published primer sequences; Collagen I (COL1A1: forward: GGACACAGAGGTTTCAGTGGT, Reverse: GCACCATCATTTCCACGAGC), Aggrecan (ACAN: forward: GCTACCCTGACCCTTCATC, Reverse: AAGCTTTCTGGGATGTCCAC), and Glyceralde-hyde-3-phosphate dehydrogenase (GAPDH: forward: GTCTCCTCTGACTTCAACAG, Reverse: GTTGTCATACCAGGAAATGAG). Gene expression values were normalised to GAPDH housekeeping gene and are presented as relative expression to 24hr time point scaffolds for each group. The $2^{-\Delta\Delta Ct}$ method was used to calculate relative mRNA levels.

2.16. Statistical analysis

Results have been presented as mean ± standard error of mean, unless stated otherwise. Statistical analysis was performed using one-way ANOVA with Tukey's post hoc test. Statistical significance are marked as * $p < 0.05$, **$P < 0.01$ and ***$p < 0.001$.

3. Results

3.1. Multizone scaffold morphology characterisation

A helix shape was printed using the cryo-printer and fibres were electrospun directly onto the surface of the helix. Combining cryo-printing and electrospinning allowed the production of scaffolds with varying zonal architecture. As confirmed by the SEM images in Fig. 1, the top zone clearly presented aligned fibres whilst the middle zone possessed randomly orientated fibres. The bottom helix zone displayed a highly porous architecture. Strand diameter variation of the printed helix was also calculated and 77% of the measurements of stand diameter ranged between 0.8 and 1.2 cm (Fig. 2A). Interestingly, the printed helix expressed 52% pores smaller than 3 µm and 47% pores ranging between 3 and 5.5 µm (Fig. 2B). Moreover, 95% of randomly orientated fibres in the middle zone were above 1.4 µm, whereas, only 61% of aligned fibres in the top zone were larger than 1.4 µm (Fig. 2C and D). The aligned fibres diameters was 1.57 ± 0.50 and the randomly orientated fibres

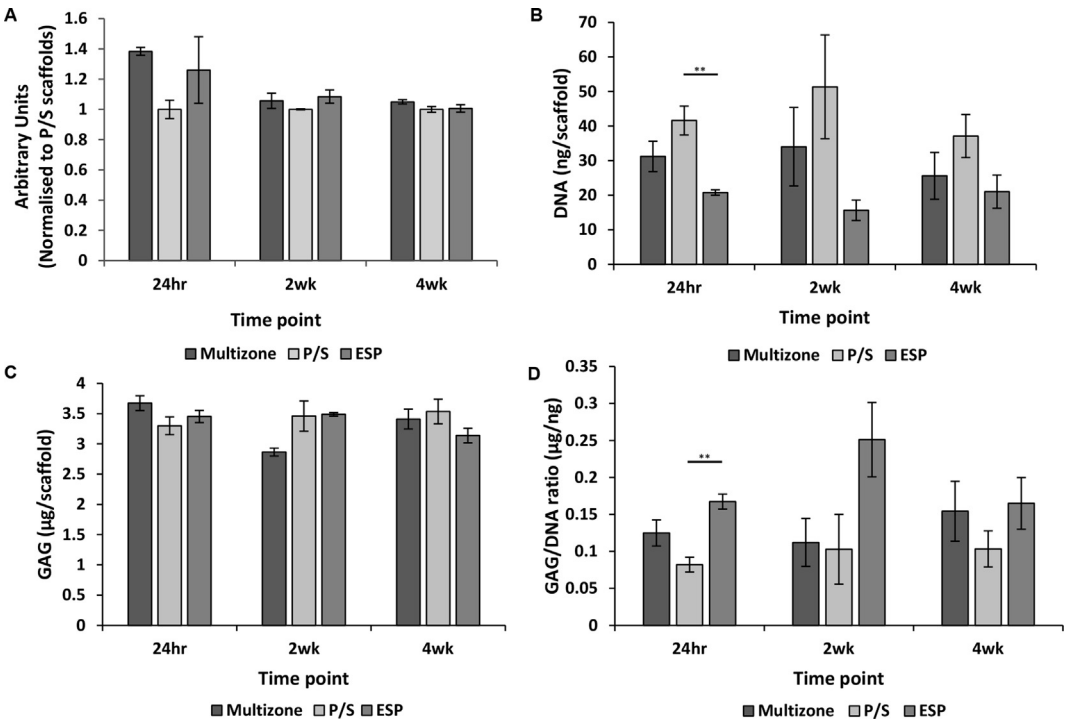

Fig. 3. Scaffold biochemical evaluation. (A) Cell viability, the fluorescence is normalised to the P/S control scaffolds at 24 h. (B) DNA quantification. (C) Sulphated GAG content. (D) GAG/DNA ratio. Error bars = Standard error mean, n = 4. Statistical significance denoted by *p < 0.05, **p < 0.01; one-way ANOVA with Tukey post hoc test.

displayed fibre diameters of 2.34 ± 0.74. The pore size of the helix bottom zone is 3.62 ± 0.32 (Fig. 2E).

3.2. Biochemical quantification

DNA quantification revealed seeding efficiencies of 64, 62 and 48% in the helix, phase separated and electrospun scaffolds, respectively, when compared to cells cultured in tissue culture plastic (Supplementary Fig. 1A). Moreover, all scaffolds demonstrated to have similar cell viability compared to cells cultured in tissue culture plastic (Supplementary Fig. 1B). The adhesion and viability of MSC on multizone scaffolds was evaluated for 24hr, 2 and 4 weeks using the CellTiter-Blue assay. The results reveal the ability of multizone scaffold to allow initial cell attachment as shown in the 24hr time point and cell viability after 2 and 4 weeks of culture (Fig. 3A). To further investigate cell adhesion, PicoGreen assay was carried out for DNA quantification (Fig. 3B). All scaffold groups demonstrated to have sustained levels of DNA after 4 weeks of culture. Both the multizone and P/S control scaffolds presented slightly higher DNA levels in comparison to the ESP control. Interestingly, GAG content and GAG/DNA ratio analysis revealed sustained levels of GAG after 4 weeks of culture in all groups (Fig. 3C and D).

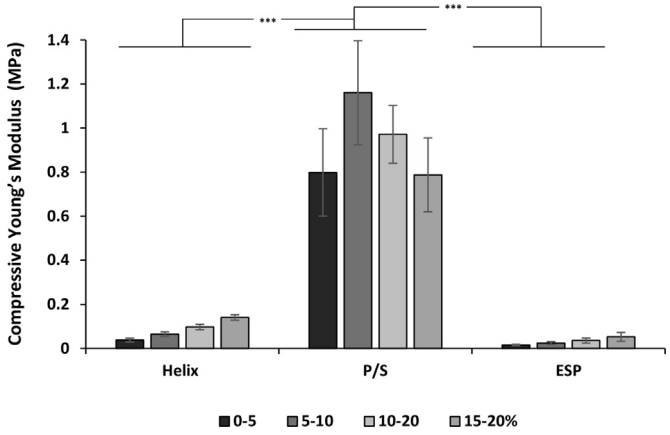

Fig. 4. Scaffolds incremental compressive Young's modulus ranging between 0 and 5, 5–10, 10–15 and 15–20% strain. Error bars = Standard error mean, n= >4. Statistical significance denoted by *p < 0.05, **p < 0.01 and ***p < 0.001; one-way ANOVA with Tukey post hoc test.

3.3. Mechanical properties

Compressive properties of scaffolds are displayed in Fig. 4. P/S control scaffolds presented to have increased compressive Young's modulus in comparison to the multizone and ESP scaffolds at all increments. Interestingly, the multizone scaffold displays a non-significant increase in Young's modulus when compared to the ESP control.

3.4. MSC staining on scaffolds

DAPI and phalloidin fluorescence staining revealed attachment of MSC on all scaffolds at 24hrs and after 4 weeks of *in vitro* culture (Fig. 5). To further investigate MSC localisation and attachment on multizone scaffolds, Z-stack projections and epi-fluorescence images were analysed. The epi-fluorescence images showed that MSC are localised within the void of the helix scaffold and directly on the surface of the middle randomly orientated electrospun layer at 24hrs (Fig. 6B). The Z-stack projections further confirmed the attachment of the MSC onto the middle randomly orientated electrospun layer after both 24hrs and 4wks of culture (Fig. 6C and D).

3.5. Gene expression

In order to investigate MSC phenotype, initial gene expression was analysed. The multizone scaffold expressed both aggrecan and Collagen I genes after 4 weeks of culture (Fig. 6E).

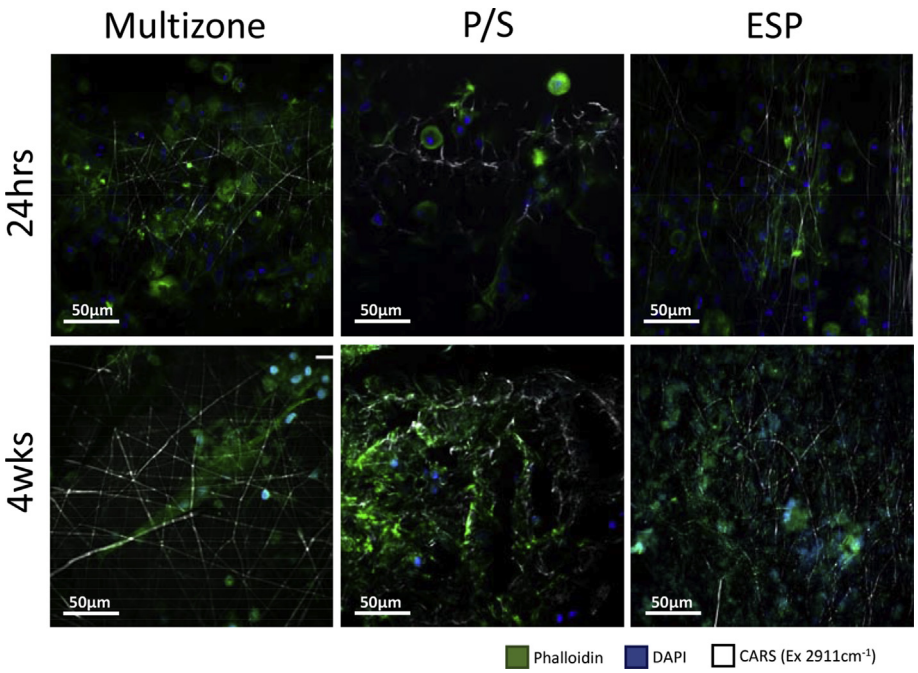

Fig. 5. MSC attachment on scaffolds shown by Two-photon excitation fluorescence (TPEF) and coherent anti-stokes Raman scattering (CARS) images after 24hrs and 4wks on multizone, phase separated (P/S) and electrospun (ESP) scaffolds.

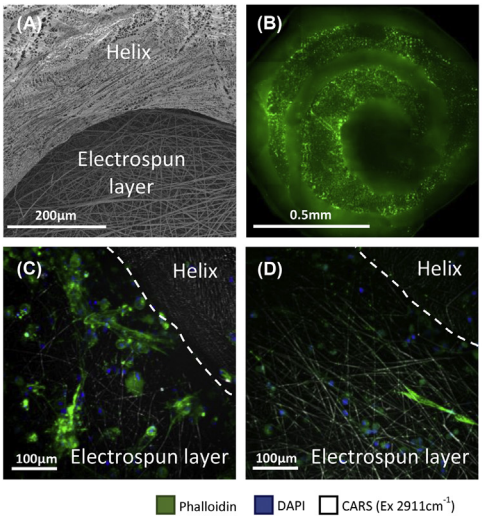

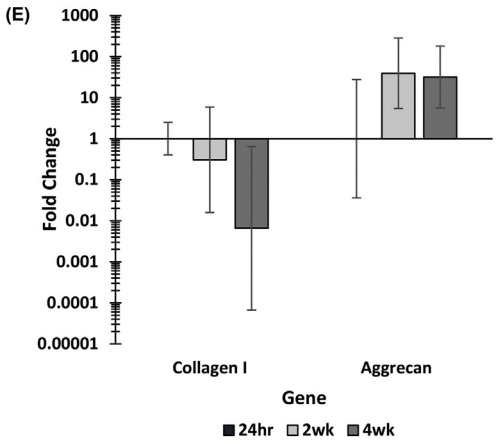

Fig. 6. Multizone scaffold characterisation. (A) SEM image of multizone scaffold. (B) Epifluorescence image of multizone scaffold showing MSC localisation within the void of helix on top of the electrospun fibres. (C) Z stack of MSC attached to multizone scaffold at 24hrs. (D) Z stack of MSC attached to multizone scaffold at 4wks. (E) Gene expression of multizone scaffolds. Values normalised to GAPDH housekeeping gene and are relative to 24hr time point gene expression. Relative expression is calculate using the $2^{-\Delta\Delta Ct}$ method. Error bars = Standard error mean, n= >3.

4. Discussion

Multizone scaffolds were fabricated with three zones, each which represents the zones of the native cartilage. MSC successfully attached to multizone scaffolds and presented viability after 4 weeks of *in vitro* culture and displayed relevant mechanical properties. PCL was used to fabricate scaffolds as it is FDA approved for use in medical devices and is well known for its biocompatible and biodegradable properties, non-toxic degradation by products and low immunogenicity [35,36]. Although PCL possesses hydrophobic nature, plasma coating can be used to overcome this. Plasma coating PCL scaffolds has been widely used to improve cell attachment [37].

ACI using *in vitro* expanded chondrocytes was the first cell based approach used for clinical osteochondral repair [2]. Research then moved on to the use of matrix assisted chondrocyte implantation [2,38]. Both techniques involve *in vitro* chondrocyte expansion and chondrocytes are known to express a low proliferation capacity. Moreover, chondrocytes lose their phenotype and dedifferentiate during monolayer expansion [39,40]. MSC are a promising alternative cell source for treating cartilage defects, as they possess high proliferation potential and multipotent properties [5,19,22]. A plethora of evidence suggests that MSC can successfully be differentiated into chondrocytes *in vitro* and the MSC differentiated chondrocytes are compatible in tissue engineering applications [22,23,41]. The present study assessed the performance of the multizone scaffolds when seeded with MSC over 4 weeks *in vitro* culture. The results of the present study clearly demonstrate the ability of multizone scaffolds to successfully allow MSC attachment, as shown by cell staining, and support cell viability over the 4 week culture period. Moreover, GAG expression was maintained over 4 weeks of culture which is key as it is the second major component of the native cartilage.

The native cartilage expresses a complex zonal architecture that is known to be responsible for various key functions of the cartilage. In the native cartilage, horizontally aligned collagen fibres in the superficial zone seamlessly transitions into randomly orientated fibres in the middle

zone, which then further transitions into vertically aligned collagen fibres in the deep zone [3,29]. This multifaceted architecture, along with unique ECM composition, allows the cartilage to present exceptional mechanical properties and provide cellular guidance by stimulating cellular function and morphology [29,42]. The important role of cartilage architecture in its functions emphasises the need to take this in to account when designing scaffolds for cartilage engineering applications. The multizone scaffold developed in this present study mimics the zonal architecture of the native cartilage. The top and middle layers of the multizone scaffold are comprised of aligned and randomly orientated electrospun fibres respectively, while the bottom zone is composed of columnar pores acquired through directional freezing. Directional freezing has been used previously to obtain structures which mimic the deep zone of the native cartilage [29,43]. Moreover, the bottom helix zone was fabricated using cryo-printing which has been previously shown to be a reproducible technique for the production of scaffolds with controlled architecture and mechanical properties [32]. In the present study, it was demonstrated that the bottom helix layer can be reproduced with low variability in the strand diameter. The void in the printed helix allows ample surface area for MSC seeding and attachment, while both electrospun fibres mimic the structural organisation of the zones in the cartilage.

Factors including interconnectivity and pore size are imperative to mediate chondrogenic differentiation, cell growth and tissue deposition. Articular cartilage is nourished via the articular fluid. Cyclic loading stimulates the movement of articular fluid through the cartilage, supplying nutrients to all zones [42,44]. The high interconnectivity and porous nature of the native cartilage allows this phenomenon to occur relatively effortlessly. Thus, when considering the structure of tissue engineered scaffolds, these factors are vital to consider. The multizone scaffolds fabricated in this study express a highly interconnected and porous structure indicating the potential for nutrients from the media to reach cells infiltrated within the scaffolds.

The native cartilage is subjected to high mechanical pressures, thus, developed scaffolds must possess the structural stability to withstand mechanical stress incurred during implantation *in vivo*. Moreover, failure of the implanted scaffold to maintain shape and structural integrity may lead to the deformation of newly formed tissue [45,46]. Likewise, high mechanical properties of scaffolds can lead to damage of the surrounding tissue, highlighting the importance of relevant mechanical properties in scaffolds [47]. The P/S control displayed relatively high compressive properties in comparison to the multizone scaffolds. This could be due to the high number of vertically aligned pores present in the scaffold. Pervious literature has suggested pore orientation is correlated with mechanical properties, in specific, vertical pores present higher compressive properties compared to horizontally aligned pores [21,29,48]. For instance, due to the helix shape, adopted for the bottom zone, the multizone scaffold has lower capacity for the production of aligned pores during the directional freezing process, thus presenting lower compressive properties than the P/S control.

Initial gene expression analysis of the multizone scaffold revealed collagen I and aggrecan expression. Low levels of collagen I is found in the native cartilage and increases during the pathogenesis of osteoarthritis [49]. However, immature cartilage during chondrocyte differentiation *in vivo* expresses high levels of collagen I and decreases as the cartilage matures [50]. On the other hand, aggrecan is a major component of the native cartilage and its expression is vital for cartilage function [42,51]. Although non-significant, a decreasing trend in collagen I expression and an increasing trend in aggrecan expression was noted during 4 weeks of *in vitro* culture. In order to investigate the full potential of these multizone scaffolds, a cell differentiation study should be carried out and detailed analysis of key differentiation gene expression should be investigated. For example the expression of collagen II, which is also a major component of the cartilage ECM, and SOX9, a key transcription factor which has a major role in several stages of chondrogenic differentiation [41]. Nonetheless, the initial gene expression shows encouraging results suggesting the potential of multizone scaffolds.

Multizone scaffolds showed cellular support when seeded with MSC. The MSC used in this present study were isolated from rat femur and a non-heterogeneous population was seeded onto the scaffolds. Donor-to-donor variability and ages of donor are two factors that which may have an influence on proliferation capacity, differentiation potential, metabolic demands and biosynthetic activity [52,53]. Future work consists on seeding these multizone scaffolds with a heterogeneous population of MSC from a more clinically relevant source, such as human derived MSC. The P/S helix in the multizone scaffold is responsible for the compressive properties of the overall scaffold. It would be interesting to further investigate the possibility of altering the helix strand thickness to control the compressive properties of the multizone scaffold. Nonetheless, the multizone scaffolds allow successful cell attachment and survival of MSC over 4 weeks of *in vitro* culture, demonstrating the potential as platforms for MSC induced cartilage ECM production.

Multizone scaffolds successfully capture the zonal architecture of the native cartilage through the use of both cryo-printing and electrospinning. The integration of techniques allowed the production of macro, micro and nano sized pores. Moreover, the mechanical properties of the multizone scaffolds were more suited for cartilage tissue applications compared to the P/S control. Multizone scaffolds supported long-term MSC attachment with the production of the essential chondrogenic biomolecule, GAG, highlighting their efficacy for MSC induced cartilage tissue engineering.

Acknowledgements

The authors would like to thank Prof. Alistair Elfick for use of lab facilities (IBioE, University of Edinburgh) and Steve Mitchell for imaging assistance (BioSEM, University of Edinburgh). This work is funded by an Engineering & Physical Sciences Research Council [EPSRC] Doctoral Training Partnership Studentship UK and Regenerative Medicine Platform II [RMPII] grant MR/L022974/1.

Appendix A. Supplementary data

Supplementary data to this article can be found online at https://doi.org/10.1016/j.bprint.2019.e00056.

References

[1] Arthritis Foundation, Arthritis by the Numbers, Arthritis Found., 2017, pp. 1–70.
[2] H.A. Breinan, T. Minas, H.-P. Hsu, S. Nehrer, S. Shortkroff, M. Spector, Autologous chondrocyte implantation in a canine model: change in composition of reparative tissue with time, J. Orthop. Res. 19 (3) (May 2001) 482–492.
[3] G.J. Delcroix, et al., Multi-layered scaffold to mimic hyaline articular cartilage architecture, Curr. Tissue Eng. 5 (2016) 21–28.
[4] D. Enea, S. Cecconi, S. Calcagno, A. Busilacchi, S. Manzotti, A. Gigante, One-step cartilage repair in the knee: collagen-covered microfracture and autologous bone marrow concentrate. A pilot study, Knee 22 (1) (2015) 30–35.
[5] R. Mardones, C.M. Jofré, J.J. Minguell, Cell Therapy and Tissue Engineering Approaches for Cartilage Repair and/or Regeneration, vol. 8, 2015, pp. 48–53, 1.
[6] G. Knutsen, et al., A randomized trial comparing autologous chondrocyte implantation with microfracture: findings at five years, J. Bone Jt. Surgery-american 89 (10) (Oct. 2007) 2105–2112.
[7] E.B. Hunziker, Articular cartilage repair: basic science and clinical progress. A review of the current status and prospects, Osteoarthritis Cartilage 10 (6) (2002) 432–463.
[8] A. Siclari, G. Mascaro, C. Gentili, R. Cancedda, E. Boux, A Cell-free scaffold-based cartilage repair provides improved function hyaline-like repair at one year, Clin. Orthop. Relat. Res. 470 (3) (2012) 910–919.
[9] R. Dorotka, U. Bindreiter, K. Macfelda, U. Windberger, S. Nehrer, Marrow stimulation and chondrocyte transplantation using a collagen matrix for cartilage repair, Osteoarthritis Cartilage 13 (8) (2005) 655–664.
[10] C. Erggelet, et al., Formation of cartilage repair tissue in articular cartilage defects pretreated with microfracture and covered with cell-free polymer-based implants, J. Orthop. Res. 27 (10) (2009) 1353–1360.
[11] J.A.M. Steele, et al., Combinatorial scaffold morphologies for zonal articular cartilage engineering, Acta Biomater. 10 (5) (2014) 2065–2075.
[12] S.D. McCullen, H. Autefage, A. Callanan, E. Gentleman, M.M. Stevens, Anisotropic fibrous scaffolds for articular cartilage regeneration, Tissue Eng. 18 (19–20) (2012) 2073–2083.

[13] M.A. Accardi, et al., Effects of fiber orientation on the frictional properties and damage of regenerative articular cartilage surfaces, Tissue Eng. 19 (19–20) (2013) 2300–2310.
[14] A. Nandakumar, A. Barradas, J. de Boer, L. Moroni, C. van Blitterswijk, P. Habibovic, Combining technologies to create bioactive hybrid scaffolds for bone tissue engineering, Biomatter 3 (2) (2013) 1–13.
[15] B.R. Mintz, J. a. Cooper, Hybrid hyaluronic acid hydrogel/poly(ε-caprolactone) scaffold provides mechanically favorable platform for cartilage tissue engineering studies, J. Biomed. Mater. Res. A 102 (9) (2014) 2918–2926.
[16] X. Wang, et al., Fabrication and characterization of poly(l-lactide-co-glycolide) knitted mesh-reinforced collagen-chitosan hybrid scaffolds for dermal tissue engineering, J. Mech. Behav. Biomed. Mater. 8 (2012) 204–215.
[17] J. Xie, et al., Articular cartilage tissue engineering based on a mechano-active scaffold made of poly(L-lactide-co-epsilon-caprolactone): in vivo performance in adult rabbits, J. Biomed. Mater. Res. B Appl. Biomater. 94 (1) (2010) 80–88.
[18] Hong Shen, Yuguang Niu, Xixue Hu, Fei Yang, Shenguo Wanga, Decheng Wu, A biomimetic 3D microtubule-orientated poly(lactide-co-glycolide) scaffold with interconnected pores for tissue engineering, J. Mater. Chem. B 3 (2015) 4417.
[19] W.J. Li, et al., A three-dimensional nanofibrous scaffold for cartilage tissue engineering using human mesenchymal stem cells, Biomaterials 26 (6) (2005) 599–609.
[20] N. Munir, A. Callanan, Novel phase separated polycaprolactone/collagen scaffolds for cartilage tissue engineering, Biomed. Mater. 13 (5) (2018), 051001.
[21] S.E. Dunphy, J.A. Reid, T.B.P. Burton, A. Callanan, Mechanical characterisation of directionally frozen polycaprolactone scaffolds using 1,4-dioxane and glacial acetic acid for articular cartilage tissue engineering, Biomed. Phys. Eng. Express 4 (5) (2018) 1–9, 057004.
[22] F. Barry, R.E. Boynton, B. Liu, J.M. Murphy, Chondrogenic differentiation of mesenchymal stem cells from bone marrow: differentiation-dependent gene expression of matrix components, Exp. Cell Res. 268 (2) (2001) 189–200.
[23] W.-J. Li, et al., A three-dimensional nanofibrous scaffold for cartilage tissue engineering using human mesenchymal stem cells, Biomaterials 26 (6) (2005) 599–609.
[24] K. Pelttari, E. Steck, W. Richter, The use of mesenchymal stem cells for chondrogenesis, Injury 39 (1) (Apr. 2008) 58–65.
[25] I.E. Erickson Bs, S.C. Van Veen, S. Sengupta, S.R. Kestle, R.L. Mauck, SYMPOSIUM: CLINICALLY relevant strategies for treating cartilage and meniscal pathology cartilage matrix formation by bovine mesenchymal stem cells in three-dimensional culture is age-dependent, Clin. Orthop. Relat. Res. 469 (10) (2011) 2744–2753.
[26] C. Acharya, et al., Enhanced chondrocyte proliferation and mesenchymal stromal cells chondrogenesis in coculture pellets mediate improved cartilage formation, J. Cell. Physiol. 227 (1) (Jan. 2012) 88–97.
[27] J. Ng, Y. Wei, B. Zhou, A. Burapachaisri, E. Guo, G. Vunjak-Novakovic, Extracellular matrix components and culture regimen selectively regulate cartilage formation by self-assembling human mesenchymal stem cells in vitro and in vivo, Stem Cell Res. Ther. 7 (183) (2016) 1–12.
[28] W.-J. Li, H. Chiang, T.-F. Kuo, H.-S. Lee, C.-C. Jiang, R.S. Tuan, Evaluation of articular cartilage repair using biodegradable nanofibrous scaffolds in a swine model: a pilot study, J. Tissue Eng. Regenerat. Med. 3 (1) (2009) 1–10.
[29] A. Arora, A. Kothari, D.S. Katti, Pore orientation mediated control of mechanical behavior of scaffolds and its application in cartilage-mimetic scaffold design, J. Mech. Behav. Biomed. Mater. 51 (2015) 169–183.
[30] J.-H. Shim, et al., Three-dimensional bioprinting of multilayered constructs containing human mesenchymal stromal cells for osteochondral tissue regeneration in the rabbit knee joint, Biofabrication 8 (1) (Feb. 2016), 014102.
[31] S. Camarero-Espinosa, B. Rothen-Rutishauser, C. Weder, E.J. Foster, Directed cell growth in multi-zonal scaffolds for cartilage tissue engineering, Biomaterials 74 (Jan. 2016) 42–52.
[32] N. Munir, R.S. Larsen, A. Callanan, Fabrication of 3D cryo-printed scaffolds using low-temperature deposition manufacturing for cartilage tissue engineering, Bioprinting 10 (Jun. 2018) e00033.
[33] X. He, L. Cheng, X. Zhang, Q. Xiao, W. Zhang, C. Lu, Tissue engineering scaffolds electrospun from cotton cellulose, Carbohydr. Polym. J. 115 (2015) 485–493.
[34] C. Vaquette, J. Cooper-White, A simple method for fabricating 3-D multilayered composite scaffolds, Acta Biomater. 9 (1) (2013) 4599–4608.
[35] L. De Franceschi, et al., Transplantation of chondrocytes seeded on collagen-based scaffold in cartilage defects in rabbits, J. Biomed. Mater. Res. A 75 (3) (2005) 612–622.
[36] T.J. Levingstone, A. Matsiko, G.R. Dickson, F.J. O'Brien, J.P. Gleeson, A biomimetic multi-layered collagen-based scaffold for osteochondral repair, Acta Biomater. 10 (5) (2014) 1996–2004.
[37] N. Abbasi, S. Soudi, N. Hayati-Roodbari, M. Dodel, M. Soleimani, The effects of plasma treated electrospun nanofibrous poly (ε-caprolactone) scaffolds with different orientations on mouse embryonic stem cell proliferation, Cell J. 16 (3) (2014) 245–254.
[38] J. Gille, E. Schuseil, J. Wimmer, J. Gellissen, A.P. Schulz, P. Behrens, Mid-term results of Autologous Matrix-Induced Chondrogenesis for treatment of focal cartilage defects in the knee, Knee Surgery Sport. Traumatol. Arthrosc. 18 (11) (2010) 1456–1464.
[39] A. Ruano-Ravina, M. Jato Díaz, Autologous chondrocyte implantation: a systematic review, Osteoarthritis Cartilage 14 (1) (Jan. 2006) 47–51.
[40] S. Reed, G. Lau, B. Delattre, D.D. Lopez, A.P. Tomsia, B.M. Wu, Macro- and micro-designed chitosan-alginate scaffold architecture by three-dimensional printing and directional freezing, Biofabrication 8 (1) (2016) 15003.
[41] R. Cai, T. Nakamoto, N. Kawazoe, G. Chen, Influence of stepwise chondrogenesis-mimicking 3D extracellular matrix on chondrogenic differentiation of mesenchymal stem cells, Biomaterials 52 (1) (2015) 199–207.
[42] A.J. Sophia Fox, A. Bedi, S.A. Rodeo, The basic science of articular cartilage: structure, composition, and function, Sport Health 1 (6) (2009) 461–468.
[43] M.W. Pot, et al., Versatile wedge-based system for the construction of unidirectional collagen scaffolds by directional freezing: practical and theoretical considerations, ACS Appl. Mater. Interfaces 7 (16) (2015) 8495–8505.
[44] V.C. Mow, P.A. Torzilli, Fundamental fluid transport mechanisms through articular cartilage, Ann. Rheum. Dis. 34 (Suppl 2) (Dec. 1975) Suppl 82–S 84.
[45] B.P. Chan, A.K.W. Leong, Scaffolding in tissue engineering: general approaches and tissue-specific considerations, Eur. Spine J. 17 (4) (2008) 467–479.
[46] G. Kim, S. Ahn, H. Yoon, Y. Kim, W. Chun, A cryogenic direct-plotting system for fabrication of 3D collagen scaffolds for tissue engineering, J. Mater. Chem. 19 (46) (2009) 8817–8823.
[47] G. Kim, S. Ahn, H. Yoon, Y. Kim, W. Chun, A cryogenic direct-plotting system for fabrication of 3D collagen scaffolds for tissue engineering, J. Mater. Chem. 19 (46) (2009) 8817–8823.
[48] C.R. Rowland, L.A. Colucci, F. Guilak, Fabrication of anatomically-shaped cartilage constructs using decellularized cartilage-derived matrix scaffolds, Biomaterials 91 (2016) 57–72.
[49] L. Zhong, X. Huang, M. Karperien, J.N. Post, Correlation between gene expression and osteoarthritis progression in human, Int. J. Mol. Sci. 17 (7) (2016) 1–14.
[50] C. Karlsson, et al., Differentiation of human mesenchymal stem cells and articular chondrocytes: analysis of chondrogenic potential and expression pattern of differentiation-related transcription factors, J. Orthop. Res. 25 (2) (Feb. 2007) 152–163.
[51] C. Kiani, L. Chen, Y.J. Wu, A.J. Yee, B.B. Yang, Structure and function of aggrecan, Cell Res. 12 (1) (Mar. 2002) 19–32.
[52] J. Fafián-Labora, et al., Influence of age on rat bone-marrow mesenchymal stem cells potential, Sci. Rep. 5 (1) (Dec. 2015) 16765.
[53] A. Sanghani-Kerai, L. Osagie-Clouard, G. Blunn, M. Coathup, The influence of age and osteoporosis on bone marrow stem cells from rats, Bone Joint Res. 7 (4) (Apr. 2018) 289–297.